Iterative finite-difference solution analysis of acoustic wave equation in the Laplace-Fourier domain

Evan Schankee Um[1], Michael Commer[1], and Gregory A. Newman[1]

1 Lawrence Berkeley National Laboratory, Berkeley, CA, 94720

ABSTRACT

We have investigated numerical characteristics of iterative solutions to the acoustic wave equation in the Laplace-Fourier (LF) domain. We transformed the time-domain acoustic wave equation into the LF domain; the transformed equation was discretized with finite differences and was solved with iterative methods. Finite-difference modeling experiments demonstrate that iterative methods require an infinitesimal stopping tolerance to accurately compute the pressure field especially at long offsets. To understand the requirement for such infinitesimal tolerance values, we analyzed the evolution of intermediate solution vectors, residual vectors, and search direction vectors during the iteration. The analysis showed that the requirement arises from the fact that in the solution space, the amplitude of the pressure field varies more than sixty orders of magnitude on the common log scale. Accordingly, we propose a rule of thumb for choosing a proper stopping tolerance value. We also examined numerical dispersion errors in terms of the grid sampling resolutions per skin depth and wavelength. We found that despite the similarity of the form of the acoustic wave and electromagnetic diffusion equations, the former is different from the latter due to the fact that in the LF domain, the skin depth of the acoustic wave equation is decoupled from its wavelength. This aspect requires that in the LF domain, its grid size be determined by considering the minimum grid sampling resolutions based not only the wavelength but also the skin depth.

INTRODUCTION

The full waveform inversion (FWI) is a seismogram-fitting imaging method through full wavefield modeling and attempts to extract quantitative information about subsurface structures (Virieux and Operto, 2009). In FWI, computationally intensive wavefield modeling has been considered a major numerical challenge although efficient modeling algorithms and massively parallel computers are increasingly available. Another difficulty associated with FWI is the convergence of the FWI misfit function toward local minimums because of the lack of reliable low-frequency data (Epanomeritakis et al., 2008; Plessix, 2009).

Recently, FWI in the frequency domain has demonstrated its capability of resolving the velocity of complex seabed and salt structures. The recent success is mainly contributed from the Laplace and the Laplace-Fourier (LF) waveform inversion methods (Shin and Cha, 2008, 2009). The Laplace and LF waveform inversion methods are utilized to construct a smooth, long-wavelength velocity model with sufficient depth coverage. The resulting smooth velocity model is used as a reliable initial model for the subsequent FWI in the frequency domain.

The Laplace and LF waveform inversion methods require solving the acoustic wave equation in the Laplace and LF domain, respectively. The transformed wave equation is discretized via finite-difference (FD) or finite-element (FE) methods into a large sparse matrix equation. When the Laplace and the LF waveform inversion methods were first formulated and evaluated, they were mainly implemented in the 2D modeling space (Cha and Shin, 2010; Shin et al, 2010). For such 2D problems, direct methods have been the method of choice for the sparse matrix equation due to their easy use and robustness. However, when a complex 3D model is simulated to interpret real field data, direct methods can be easily hindered by their large memory requirements and difficulties for their efficient parallel implementation (Golub and Loan, 1996). Accordingly, recent studies on 3D acoustic waveform inversion in the Laplace domain have been carried out using an iterative method (Pyun et al., 2011).

Numerical characteristics of iterative solution processes to the acoustic wave equation in the Laplace and LF domain have not yet been investigated. One might predict strong similarities of

numerical characteristics between the acoustic wave equation in the LF domain and the electromagnetic (EM) diffusion equation in the frequency domain. This prediction would be based on the fact that a damping constant and a Fourier frequency in the LF domain can be conceptually compared to the electrical conductivity and the source frequency in EM, respectively. However, despite similarities, as demonstrated in this paper, numerical characteristics of the acoustic wave equation are different from those of the EM diffusion equation. For example, iterative FD solutions to the acoustic wave equation in the LF domain require an infinitesimal stopping tolerance value to ensure the accuracy especially at long source-receiver offsets. A discretization of the wave equation in the LF domain is also different from that of the EM diffusion equation.

Here, we investigate numerical characteristics of iterative solution processes to the acoustic wave equation in the Laplace and LF domain. In fact, because the Laplace transform is the equivalent of the LF transform with zero Fourier frequency (Lathi, 2005), the Laplace transform can be considered as a subdomain of the LF domain. Therefore, in this paper, we do not distinguish the LF domain from the Laplace domain. The remainder of this paper is organized as follows. First, we review the acoustic wave equation in the LF domain and its 3D FD solution approach. We also briefly compare the acoustic wave equation in the LF domain with the EM diffusion equation in the frequency domain. The comparison hopefully leads to understanding of the differences and similarities between the two equations. Second, we examine effects of the tolerance of iterative methods on the accuracy of solutions to the acoustic wave equation as a function of offset. We follow this by examining LF modeling parameters that influence the convergence rate of the FD solution. Next, we analyze numerical dispersion errors of the 3D FD solution. By carrying out the analysis, we provide a rule of thumb to determine an economic grid size for 3D FD modeling of the acoustic wave equation in the LF domain.

ACOUSTIC WAVE EQUATION IN THE LF DOMAIN

The acoustic wave equation in the time domain for an unbounded, homogeneous and isotropic medium (Marfurt, 1984; Cohen, 2001) is

$$-\nabla^2 p(\mathbf{r},t) + \frac{1}{V^2}\frac{\partial p(\mathbf{r},t)}{\partial t^2} = s(\mathbf{r},t), \tag{1}$$

where V is the velocity, $\mathbf{r}$ is a position vector, t is time, $p(\mathbf{r},t)$ is the pressure field at $(\mathbf{r},t)$, and $s(\mathbf{r},t)$ is the source term.

The LF transform of the pressure field (Shin and Cha, 2009) is given as

$$\hat{p} = \hat{p}(\mathbf{r},\sigma,\omega) = \int_0^\infty p(\mathbf{r},t)e^{-(\sigma+i\omega)t}dt, \tag{2}$$

where σ and ω are a Laplace damping constant and an angular Fourier frequency, respectively.

The LF transform of equation 1 yields

$$-\nabla^2\hat{p} + k^2\hat{p} = \hat{s}, \quad \text{where wave number } k = -\frac{\sigma+i\omega}{V}. \tag{3}$$

Because the eigenfunction of the differential operator of equation 3 (Courant and Hilbert, 1989) is e^{kx}, a skin depth that is defined as the distance at which the pressure field is attenuated to $1/e$ of its original amplitude and a wavelength are given as

$$\text{skin depth } \delta = \frac{V}{\sigma}; \tag{4}$$

$$\text{wavelength } \lambda = \frac{V}{f}, \text{ where } f \text{ is a Fourier frequency.} \tag{5}$$

The skin depth and the wavelength are utilized later as primary parameters for grid design through numerical dispersion analysis.

At this point, it is instructive to compare the skin depth and the wavelength of the acoustic wave equation in the LF domain with those of the EM diffusion equation in the frequency domain. For a given velocity in the LF domain, the skin depth and the wavelength are solely controlled by the damping constant and the Fourier frequency, respectively. In other words, the damping constant does not affect the wavelength. Neither does the Fourier frequency affect the skin depth. Because both the skin depth and the wavelength independently describe the spatial change of the pressure field, one must consider both together in designing FD grids in the LF domain. We will demonstrate this aspect using 3D FD models later. In contrast to the damping constant, an electric conductivity, which is logical to be compared to the damping constant in the LF domain because both are responsible for the attenuation, affects both the skin depth and the wavelength (Appendix A). In fact, the wavelength (equation A-5) of the EM field is simply given as 2π times the skin depth (equation A-4), indicating that the skin depth and the wavelength basically serve as the same yardstick to measure the spatial change of EM fields. Therefore, one can consider either of them for its FD grid design.

To derive an FD scheme for the acoustic wave equation, we discretize equation 3 in the 3D space using a second-order central difference scheme. A zero-pressure boundary condition (Keys, 1985) is applied to the air-earth interface. A one-way wave equation (Engquist and Majda, 1977) is applied to other computational boundaries. The resulting sparse matrix equation is given as

$$\mathbf{Mp} = \mathbf{s}, \tag{6}$$

where $\mathbf{M}$ is a system matrix, $\mathbf{p}$ is an unknown vector of the pressure field, and $\mathbf{s}$ is a source vector which corresponds to an impulse source in the time domain.

In general, the system matrix is complex, symmetric, and non-Hermitian. Therefore, we solve equation 6 using a quasi-minimal residual (QMR) method (Freund, 1992). For the QMR method to converge effectively, the Jacobi preconditioner (Barrett et al., 1994) is employed. As a side note, when the Fourier frequency is set to zero, the system matrix becomes symmetric and positive definite. In this case, a conjugate gradient (CG) method can also be the method of choice for equation 6 (Hestenes and Stiefel, 1952). In our FD scheme, the initial guess of the solution to equation 6 is set to a zero vector. Our FD scheme is also implemented on massive parallel computers using the Message Passing Interface (Commer et al., 2008). The parallel implementation allows us to simulate sufficiently large spatial distances. In the next section, along the long survey line, we demonstrate an extremely large dynamic range of the solution to equation 6 with typical LF modeling parameters (i.e., a damping constant and a Fourier frequency). We investigate the

effects of a stopping tolerance on the FD solution accuracy as a function of a source-receiver offset.

NUMERICAL CHARACTERISTICS OF ITERATIVE FD SOLUTIONS

To illustrate the effect of the stopping tolerance on the accuracy of the FD solution, we solve the acoustic wave equation for a simple 3D homogeneous whole-space seawater model. The velocity of the model is set to 1500 m/s. A damping constant and a Fourier frequency are set to 10 and 0, respectively. The FD model is discretized with 15 m uniform grid cells and consists of $1734 \times 667 \times 667$ grid cells in the x-, y-, and z-directions (we will discuss in the next section how to determine a proper grid size when a velocity, a damping constant, and a Fourier frequency are given). The source is placed at $x = 0$ m. The maximum source-receiver offset is set to 20 km.

The iterative FD solutions to this model are computed with a stopping tolerance varying from 10^{-30} to 10^{-130} and are compared with a corresponding analytic solution. As shown in Figure 1a, the pressure field decays rapidly due to the damping constant. As a result, along the survey line, the pressure field varies more than sixty orders of magnitude. Although the acoustic wave equation is frequently compared to the EM potential or diffusion equation, this extremely wide dynamic range is not observed in EM problems. For example, in controlled-source EM modeling, a typical dynamic range of EM solutions are smaller than 10 orders of magnitude (Um and Alumbaugh, 2007; Chave, 2009). As investigated below, this extremely wide dynamic range of the pressure field in the LF domain differentiates the iterative solution processes compared to the EM diffusion equation in the frequency domain.

Figure 1a indicates that a smaller tolerance is required to accurately compute smaller pressure fields at longer offsets. We assume that the FD solutions to equation 3 are sufficiently accurate if their relative errors (Figure 1b) with respect to the analytical solution are less than 5%. For example, when the tolerance is set to 10^{-30}, the iterative solution produces the accurate pressure field only before $x = 4.4$ km. Beyond $x = 4.4$ km, the pressure field remains close to the initial guess of zero, implying that the pressure field does not seem to be updated during iterative processes. As a result, the relative errors quickly increase beyond $x = 4.4$ km. Due to the logarithmic scale used for the pressure field axis, the near-zero-pressure field is not plotted beyond $x = 6$ km. Figure 1 demonstrates that for the QMR method to accurately compute the pressure field up to $x = 20$ km, the tolerance should be reduced to 10^{-130}.

To understand why such an infinitesimal tolerance value is required for accurately computing the pressure field at long offsets, we further simplify the model above by considering the 1D acoustic wave equation. Because iterative FD solution processes of the 1D equation require a much smaller amount of memory than that of the 3D equation, we store an intermediate solution vector, a residual vector, and a search direction vector during the iteration. The analysis of the evolution of these vectors elucidates the mechanism of the iterative solution construction, helping us understand the requirement for the infinitesimal tolerance. An FD scheme for the 1D equation is also formulated using a second-order central difference and one-way wave equation boundary conditions. In the 1D model, the damping constant, the Fourier frequency, the velocity, and the grid size are set to the same as those in the 3D model above. Because the Fourier frequency is set to zero, the 1D model is solved using the CG method.

Figure 2 shows the evolution of intermediate solution vectors, residual vectors and CG search direction vectors at selected iteration steps. The residual and search direction vectors are projected onto a part of the solution space that is covered by the 20-km-long source-receiver offset. First, we examine the behavior of the three vectors at the 10th iteration step. The 10th residual vector has its largest element in the solution space near the source position (Figure 2b). In contrast, in the remaining solution space, the residual vector has near-zero elements. The largest element is created around the source in the solution space because the pressure amplitude is the largest at the source position and decays very rapidly with increasing offset. Because the CG method optimally minimizes a norm of the residual vector in the given Krylov subspace, it chooses the search direction vector such that the largest element in the residual vector can be effectively reduced. As a result, the search direction vector effectively spans only a small portion of the solution space where the

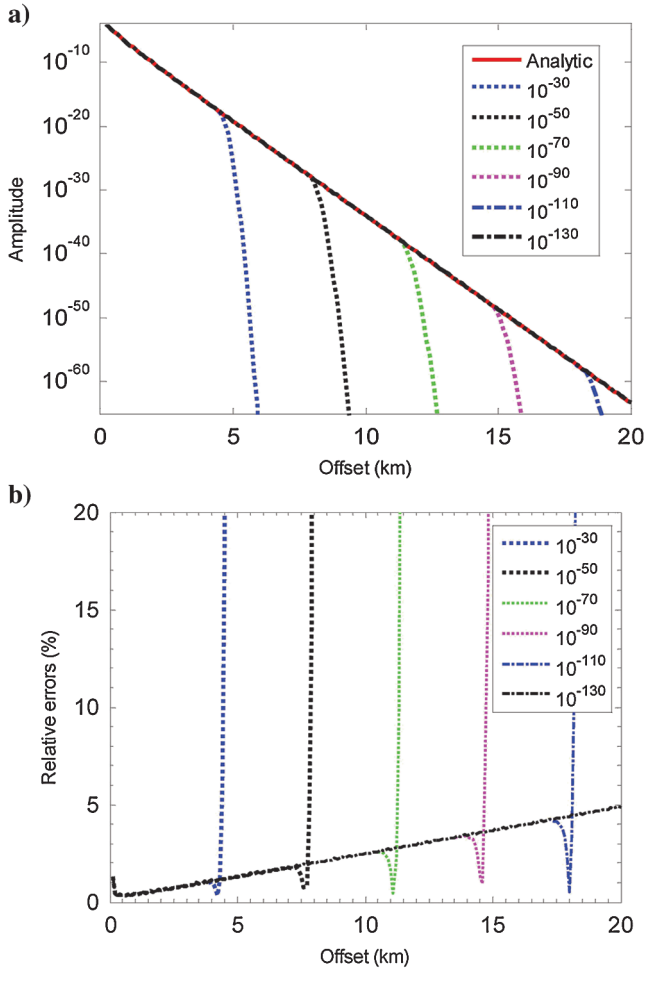

Figure 1. (a) Three-dimensional FD solutions of the acoustic wave equation in the LF domain for the homogeneous whole-space model with a velocity of 1500 m/s. The source is placed at $x = 0$ m. The survey line (the x-axis) is 20 km long. The six stopping tolerance values ranging from 10^{-30} to 10^{-130} are used to demonstrate the accuracy of the FD solutions via the QMR method. (b) Relative errors of the FD solutions with respect to the analytic solutions.

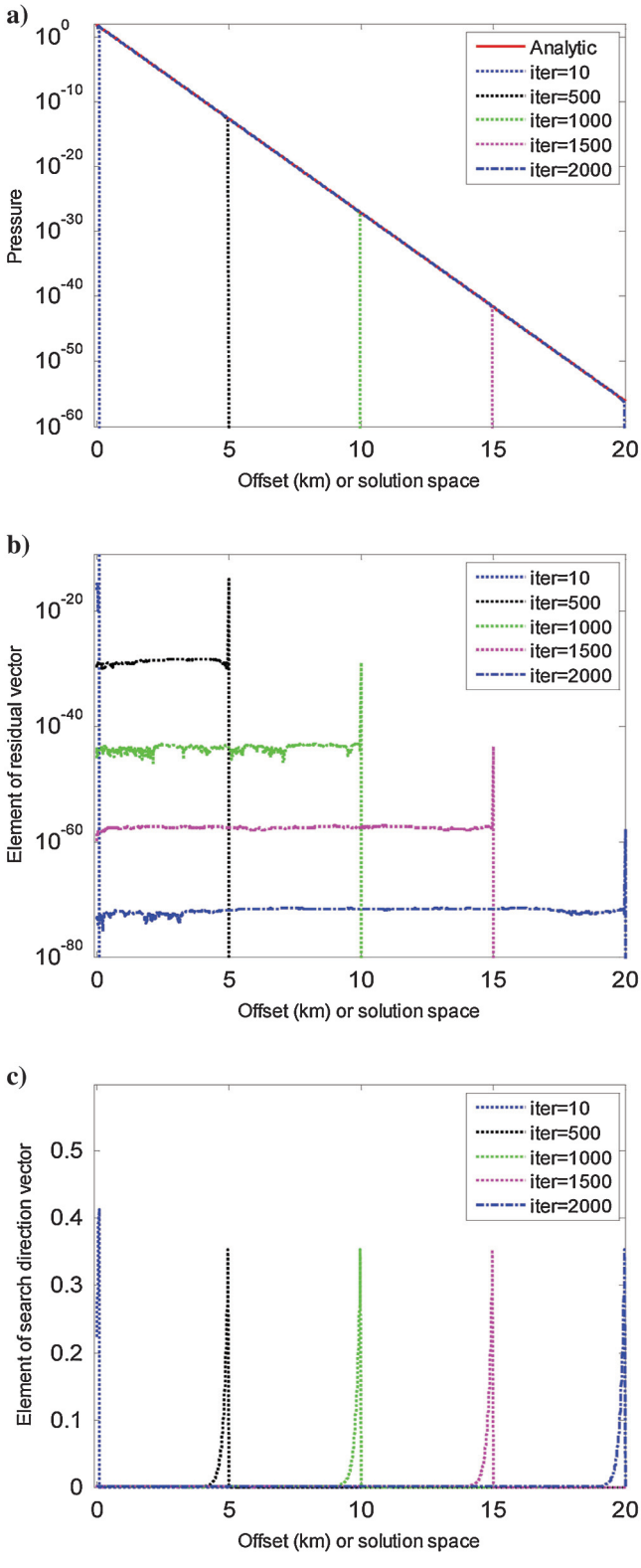

Figure 2. The evolution of (a) intermediate solution vectors, (b) residual vectors, and (c) search direction vectors. In (a), the elements of the intermediate solution vectors smaller than 10^{-60} are not plotted. In (b), the elements of the residual vectors smaller than 10^{-80} are not plotted.

largest elements of the residual reside (Figure 2c). Therefore, the other part of the solution is not effectively updated and remains close to the initial value (i.e., zero). For example, after the 10th iteration step, the intermediate FD solution corresponds to the analytic solution only around the source position (Figure 2a).

As the iteration continues, the largest element of the residual vector gradually migrates outward from the source position (Figure 2b). So does the solution space that the corresponding search direction vector effectively spans (Figure 2c). Accordingly, the accuracy of the intermediate solutions gradually improves over a larger offset (Figure 2a). Consequently, the stopping tolerance should be sufficiently small to allow extra iteration steps at which the search direction vectors span the solution space associated with large offsets. The stopping tolerance should also be small enough such that the infinitesimal amplitude of the pressure fields at the largest offset can be considered when a stopping criterion is evaluated.

As shown in Figures 1 and 2, a proper tolerance value strongly depends on the maximum offset to be simulated. Based on our

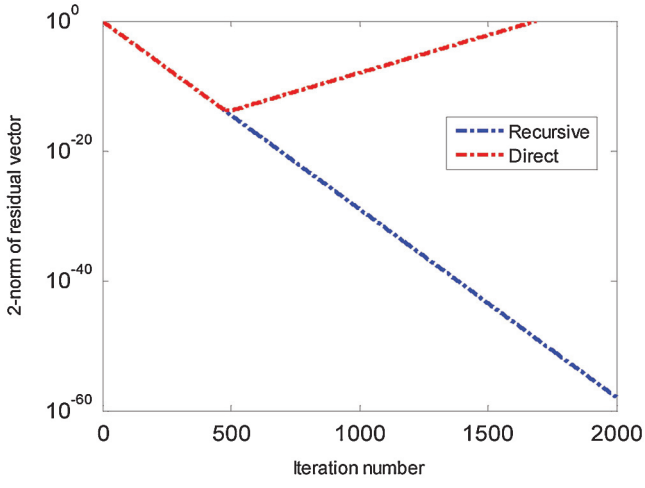

Figure 3. The 2-norm comparison of the recursively computed and directly computed residual vectors.

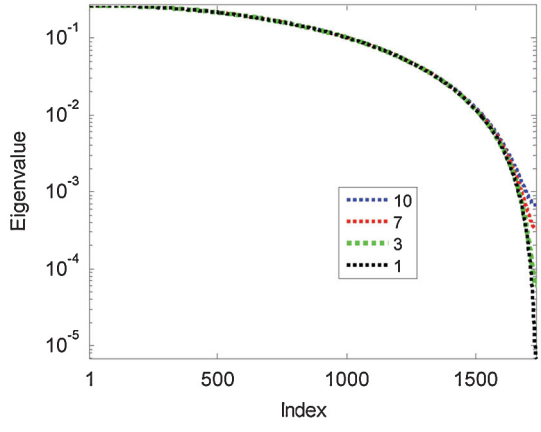

Figure 4. The eigenvalue distribution of the system matrix of equation 6 for the 1D acoustic wave equation with four damping constants: 10, 7, 3, and 1. The Fourier frequency is set to 0 Hz.

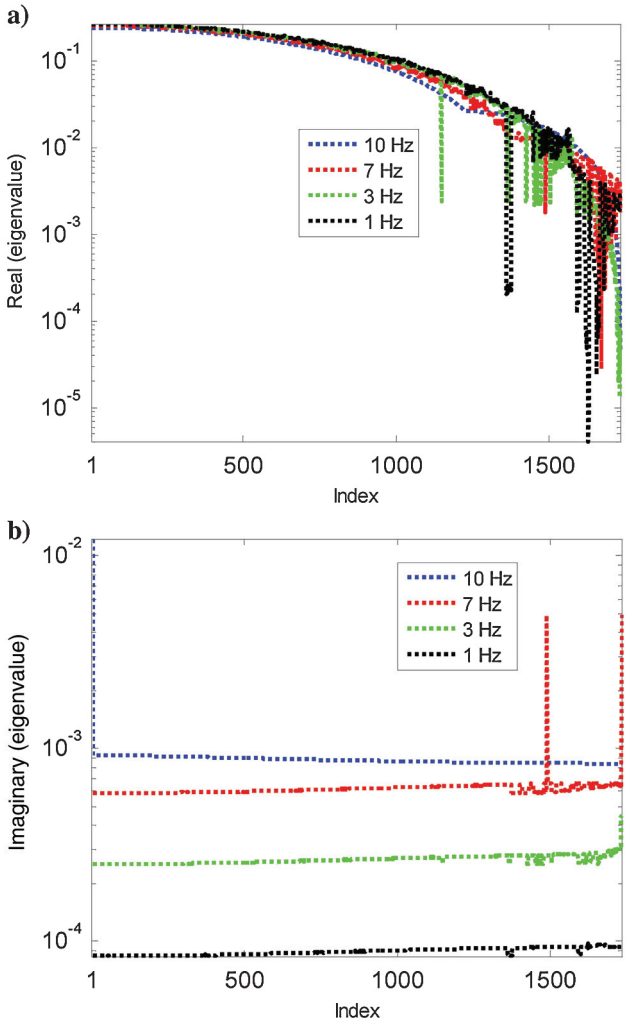

Figure 5. The eigenvalue distribution of the system matrix of equation 6 for the 1D acoustic wave equation with four Fourier frequencies. The damping constant is set to one. (a) The real component of eigenvalues. (b) The imaginary component of eigenvalues.

extensive 3D FD modeling experiments, our rule of thumb for choosing a small enough stopping tolerance is to set it to be slightly smaller than the square of the minimum amplitude of the pressure fields that is typically recorded at the largest offset. For example, as shown in Figure 1, the QMR method produces the accurate solution up to $x = 20$ km when the tolerance is set to 10^{-130} which is slightly smaller than the square of the pressure amplitude (i.e., 10^{-64}) at $x = 20$ km. For a complex 3D model, one can roughly estimate the minimum amplitude from a 1D background model.

To use such an infinitesimal tolerance value in the iterative methods, one should compute the residual vector by recursively updating previous residual vectors (Freund, 1992) rather than by directly evaluating the residual vector $\mathbf{r}^i = \mathbf{M}\mathbf{p}^i - \mathbf{s}$, where the superscript i denotes the ith iteration step. It is known that a norm of the recursively updated residual vector can be many orders of magnitude smaller than a given machine precision (Greenbaum, 1997). In contrast, a norm of the directly computed residual vector does not decrease below the machine precision and can even increase due to round-off errors. Thus, the norm of the directly computed residual vector makes the iteration stop too soon before the pressure field is accurately computed at long offsets. For example, the 2-norm of a recursively computed residual vector (Barrett et al., 1994) of the 1D model is compared with that of the directly computed residual vector in Figure 3. The former linearly decreases on the log scale, whereas the latter reaches about 10^{-14} and starts to increase with additional iterations. Consequently, iterative methods that utilize a directly computed residual vector (e.g., a preconditioned CG routine in MATLAB) are stopped at 484 iterations.

Next, using the 1D model, we investigate the impact of the damping constant and the Fourier frequency on clustering of eigenvalues that is directly related to the convergence rate of an iterative method. Figure 4 shows the eigenvalue distribution of system matrix of equation 6 as a function of the damping constant. As the damping constant decreases, small eigenvalues are increasingly less clustered. The corresponding condition number of the system matrix gradually increases from 401.0, 817.3, 4445.4, to 3999.4. Therefore, as demonstrated in the next section, equation 6 with a smaller damping constant requires more iteration steps for the convergence although a relatively larger stopping tolerance is provided.

The impacts of the Fourier frequency on clustering eigenvalues are demonstrated in Figure 5. As the Fourier frequency decreases, the eigenvalues become less clustered. When the Fourier frequency

Table 1. The summary of the modeling parameters and errors with a damping constant varying from one to 10. For each damping constant, the minimum amplitude of the pressure field along the survey line is analytically calculated and is used to set up a small enough stopping tolerance.

Model no.	V (km/s)	σ	f (Hz)	λ (m)	δ (m)	Δx (m)	N_λ	N_δ	Min. amp. of pressure (1D)	QMR tolerance	No. of iterations	Max. error (%)
1	1.5	1	3	500	1500	50	10	30	7.4×10^{-12}	10^{-30}	1664	1.9
2	1.5	2	3	500	750	50	10	15	1.2×10^{-17}	10^{-50}	1470	2.8
3	1.5	3	3	500	500	50	10	10	2.0×10^{-23}	10^{-60}	1163	3.2
4	1.5	4.5	3	500	333	50	10	6.7	3.5×10^{-32}	10^{-80}	1041	2.2
5	1.5	6	3	500	250	50	10	5	1.1×10^{-40}	10^{-100}	982	4.2
6	1.5	10	3	500	150	50	10	3	4.9×10^{-64}	10^{-130}	772	60

decreases from 10, 7, 3, and 1, the corresponding condition number increases from 572.3, 859.3, 2088.6, to 6276.8. Accordingly, the convergence rate gradually decreases. In short, smaller damping constants and Fourier frequencies tend to decrease the convergence rate. However, based on our 3D FD modeling experiments, we conclude that the simple Jacobi preconditioner works reasonably well for equation 6 with a typical range of damping constants (one to 10) and Fourier frequencies (0 to 10 Hz).

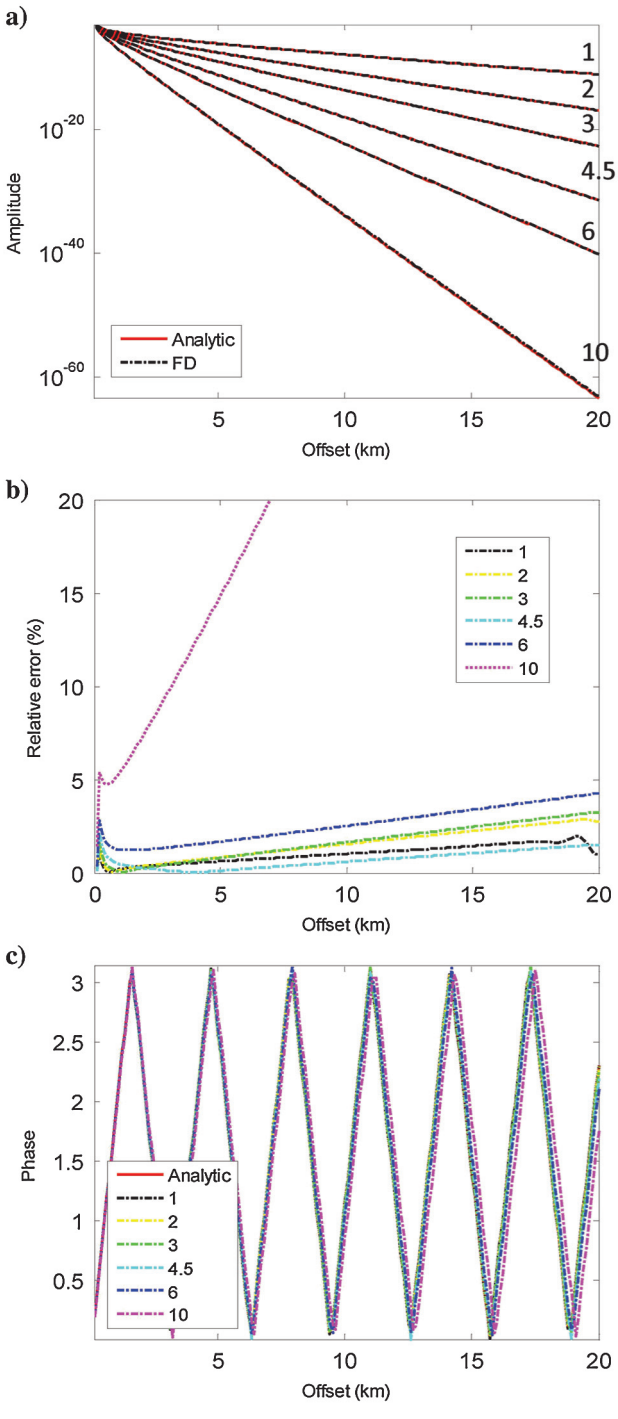

Figure 6. (a) The amplitude of the pressure field, (b) the relative errors of the amplitude of the pressure field, and (c) the phase of the pressure field is plotted as a function of the source-receiver offset and the damping constant that varies from one to 10. The Fourier frequency is set to 3 Hz. For detailed modeling parameters, see Table 1.

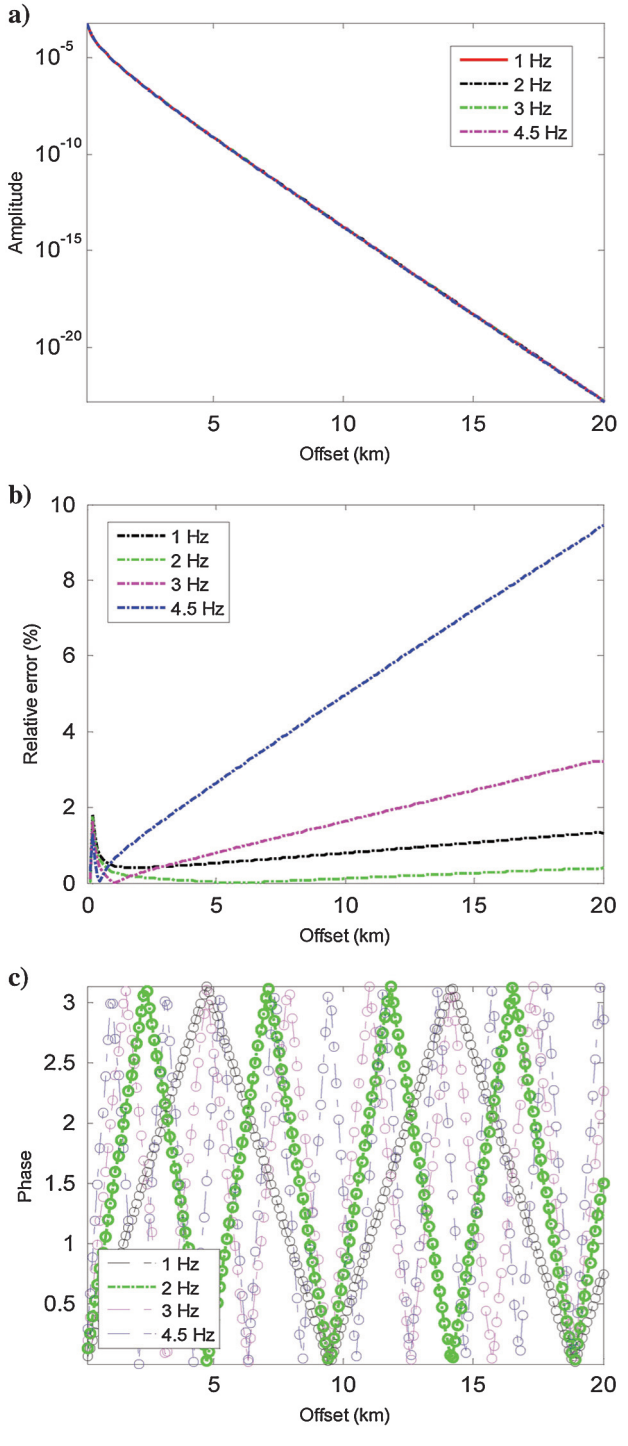

Figure 7. (a) The amplitude of the pressure field, (b) the relative errors of the amplitude of the pressure field, and (c) the phase of the pressure field is plotted as a function of the source-receiver offset and a Fourier frequency that varies from one to 10. In (c), the broken lines and the broken lines with circles denote the analytic and FD solutions, respectively. In (a), (b), and (c), the damping constant is set to three. For detailed modeling parameters, see Table 2.

Table 2. The summary of the modeling parameters and errors with a Fourier frequency varying from one to 4.5.

Model no.	V (km/s)	σ	f (Hz)	λ (m)	δ (m)	Δx (m)	N_λ	N_δ	Min. amp. of pressure (1D)	QMR tolerance	No. of iterations	Max. error (%)
7	1.5	3	1	1500	500	50	30	10	2.0×10^{-23}	10^{-30}	1125	1.3
8	1.5	3	2	750	500	50	15	10	2.0×10^{-23}	10^{-30}	1152	0.4
9	1.5	3	3	500	500	50	10	10	2.0×10^{-23}	10^{-23}	1173	3.2
10	1.5	3	4.5	333	500	50	6.7	10	2.0×10^{-23}	10^{-30}	1197	9.4

NUMERICAL DISPERSION ANALYSIS

So far, we have investigated numerical characteristics of solving the acoustic wave equation in the LF domain using iterative methods. The use of iterative methods improves the overall computational efficiency because they not only require a relatively small amount of memory but also can be effectively parallelized. To further improve the computational efficiency, it is also important to economically discretize a given computational domain. A too dense discretization results in storage and computational overhead, whereas a too coarse discretization causes inaccurate solutions and unacceptable numerical dispersion errors. In this section, we determine a proper grid size by systematically exploring the effects of modeling parameters on the solution accuracy. As described before, we assume that FD solutions to equation 3 are accurate enough if their relative errors with respect to the corresponding analytical solutions are within about 5%. Because the degree of the numerical dispersion increases with the source-receiver offset, we consider this error limit within the 20 km offset which is sufficiently longer than a typical survey line.

First, we consider the homogeneous whole-space seawater model whose velocity is 1500 m/s. A Fourier frequency is fixed to 3 Hz, whereas a damping constant varies from one to 10. The 50-m uniform FD grids are used to simulate the pressure field. The modeling parameters are summarized in Table 1. The resulting amplitude and phase of the pressure field are plotted in Figure 6. As the damping constant increases, the amplitude of the pressure field is more rapidly attenuated as a function of the offset (Figure 6a). The higher a damping constant is used, the larger spatial gradient of the pressure field develops. Therefore, a finer FD grid should be used to resolve such rapid change of the pressure field. Because a grid size is constant in the models, the accuracy of the solution gradually deteriorates with an increasing damping constant (Figure 6b). Because the skin depth is a measure of the attenuation, a proper grid size can be determined by the grid sampling resolution per skin depth, N_δ (Table 1). Based on extensive numerical experiments, we have found that our FD solutions are accurate when N_δ is approximately larger than six. When a model consists of complex velocity structures, it is recommended to use the smallest velocity value in the model for N_δ. Next, we examine the grid sampling resolution per the wavelength (N_λ). For this numerical experiment, the damping constant is fixed to three, and the Fourier frequency varies from 1 to 4.5 Hz. The modeling parameters and the modeling results are summarized in Table 2 and Figure 7, respectively. Our numerical modeling experiments suggest that for accurate solutions, N_λ should be approximately larger than 10 for our second-order differencing scheme. At this point, it is instructive to mention that a classic finite-difference time-domain (FDTD) formulation of the acoustic wave equation (Alford et al., 1974) requires a similar rule of thumb for determining a proper grid size (e.g., $N_\lambda > 10$) However, in contrast to the FDTD formulation, a FD grid size in the LF domain should be chosen to satisfy both minimum N_δ and N_λ.

Figures 6 and 7 also graphically elucidate the requirement for both N_δ and N_λ. When the Fourier frequency is fixed, the damping constant controls only the attenuation of the pressure field (Figure 6a). the wavelength does not change as inferred from the phase plots (Figure 6c). In contrast, for the constant damping constant, the Fourier frequency controls only the wavelength as inferred from the phase plots (Figure 7c). Thus, the amplitude of the wavefield does not change (Figure 7a). In short, the skin depth is completely decoupled with the wavelength. One must consider both minimum N_δ and N_λ to determine an accurate grid size. In addition to an extremely wide dynamic range of the pressure field in the LF domain, this decoupling aspect is another major difference between the acoustic wave equation in the LF domain and the EM diffusion equation in the frequency domain.

Finally, Tables 1 and 2 demonstrate that behaviors of the iterative solution to the 3D problems are consistent with our previous analysis on the 1D problem. A larger damping constant requires a smaller stopping tolerance for accurate solutions. However, this requirement does not increase the total number of iteration steps for the convergence. This paradox can be explained by the observation that a larger damping constant makes eigenvalues more clustered and reduces the condition number of the system matrix. As shown in Tables 1 and 2, a sufficiently small stopping tolerance can be determined by using the minimum amplitude of the pressure field at the maximum source-receiver offset.

CONCLUSIONS

Numerical characteristics of iterative FD solutions to the acoustic wave equation in the LF domain have been investigated. An important feature of the pressure field in the LF domain is that its amplitude can be rapidly attenuated in the space and becomes infinitesimal at long offset. To ensure accurate solutions of the wave equation at long offset, iterative methods require a stopping tolerance value that is several tens of orders of magnitude smaller than a machine precision. To utilize such an infinitesimal tolerance value, a residual vector of the iterative methods should be computed recursively.

Numerical dispersion errors of iterative FD solutions have been examined. We have shown that the skin depth of the acoustic wave equation in the LF domain is decoupled from the wavelength.

Therefore, both the skin depth and the Fourier frequency independently influence the numerical dispersion errors. For accurate solutions, the minimum grid sampling resolutions per both the skin depth and the wavelength should be considered simultaneously. Lastly, we should mention that this analysis is based on the second-order FD scheme. If a higher-order FD scheme is employed, the minimum grid sampling rules are expected to be relaxed, but specific guidelines would still need to be reexamined. However, we believe our approach to numerical dispersion analysis using both the wavelength and the skin depth will still be effective and useful. We are considering implementing high-order FD schemes and investigating their impacts on reduction in numerical dispersion errors and extra computational costs incurred.

ACKNOWLEDGMENTS

This work was carried out at Lawrence Berkeley Laboratory with funding provided by the U.S. Department of Energy Office of Science and the Geothermal Program Office, under respective contract numbers DE-AC02-05CH11231 and GT-480010-19823-10. We thank Jonas D. De Basabe, two other anonymous reviewers, and editors for their useful suggestions to improve this paper.

APPENDIX A

THE WAVE LENGTH AND THE SKIN DEPTH OF THE EM DIFFUSION EQUATION IN THE FREQUENCY DOMAIN

For a source-free, homogeneous region, the electric field diffusion equation (Nabighian, 1997) is given as

$$\nabla^2\mathbf{E} + k^2\mathbf{E} = 0. \tag{A-1}$$

Note that the form of equation A-1 is basically the same as that of equation 3. The wavenumber of the diffusion equation, k is different from that of equation 3 and is given as

$$k = \sqrt{-i\omega\mu\sigma}, \tag{A-2}$$

where ω, μ, σ, and i are the angular frequency, the magnetic permeability, the electric conductivity and $\sqrt{-1}$, respectively.

For a sinusoidal time dependence e^{iwt}, the solution of equation A-1 that diffuses in the positive z-direction can be written as

$$E = E_o e^{-\beta z} e^{(\omega t - \alpha z)i}, \quad \text{where } \alpha = \beta = \sqrt{\frac{\omega\mu\sigma}{2}}. \tag{A-3}$$

Therefore, the skin depth and the wavelength of the diffusive electric field is given as

$$\text{skin depth } \delta = \sqrt{\frac{2}{\omega\mu\sigma}}; \tag{A-4}$$

$$\text{wavelength } \lambda = 2\pi\delta. \tag{A-5}$$

In short, the wavelength can be obtained by scaling the skin depth.

REFERENCES

Alford, R., K. Kelly, and D. Boore, 1974, Accuracy of finite-difference modeling of the acoustic wave equation: Geophysics, **39**, 834–842, doi: 10.1190/1.1440470.

Barrett, R., M. Berry, T. F. Chan, J. Demmel, J. Donato, J. Dongarra, V. Eijkhout, R. Pozo, C. Romine, and H. Van der Vorst, 1994, Templates for the solution of linear systems: Building blocks for iterative methods: SIAM.

Cha, Y., and C. Shin, 2010, Two-dimensional Laplace-domain waveform inversion using adaptive meshes: An experience of the 2004 BP velocity-analysis benchmark data set: Geophysical Journal International, **182**, 865–879, doi: 10.1111/(ISSN)1365-246X.

Chave, A., 2009, On the electromagnetic fields produced by marine frequency domain controlled sources: Geophysical Journal International, **179**, 1429–1457, doi: 10.1111/gji.2009.179.issue-3.

Cohen, G., 2001, Higher-order numerical methods for transient wave equations: Springer.

Commer, M., G. A. Newman, J. J. Carazzone, T. A. Dickens, K. E. Green, L. A. Wahrmund, D. E. Willen, and J. Shiu, 2008, Massively-parallel electrical-conductivity imaging of hydrocarbons using the Blue Gene/L supercomputer: First Break, **26**, 93–102.

Courant, R., and D. Hilbert, 1989, Methods of mathematical physics, Volume **1**: Wiley-VCH.

Engquist, B., and A. Majda, 1977, Absorbing boundary conditions for the numerical simulation of waves: Mathematics of Computation, **31**, 629–651, doi: 10.1090/S0025-5718-1977-0436612-4.

Epanomeritakis, I., V. Akcelik, O. Ghgattas, and J. Bielak, 2008, A Newton-CG method for large-scale three-dimensional elastic full-waveform seismic inversion: Inverse Problems, **24**, 034015, doi: 10.1088/0266-5611/24/3/034015.

Freund, R., 1992, Conjugate gradient type methods for linear systems with complex symmetric coefficient matrices: SIAM Journal on Scientific and Statistical Computing, **13**, 425–448, doi: 10.1137/0913023.

Golub, G. H., and C. F. Van Loan, 1996, Matrix computation, 3rd ed.: Johns Hopkins University Press.

Greenbaum, A., 1997, Estimating the attainable accuracy of recursively computed residual methods: SIAM Journal on Matrix Analysis and Applications, **18**, 535–551, doi: 10.1137/S0895479895284944.

Hestenes, M. R., and E. Stiefel, 1952, Methods of conjugate gradients for solving linear systems: Journal of Research of the National Bureau of Standards (United States), **49**, 409–435.

Keys, R. G., 1985, Absorbing boundary conditions for acoustic media: Geophysics, **50**, 892–902, doi: 10.1190/1.1441969.

Lathi, B. P., 2005, Linear systems and signals, 2nd ed.: Oxford.

Marfurt, J. K., 1984, Accuracy of finite-difference and finite-element modeling of the scalar and elastic wave equations: Geophysics, **49**, 533–549, doi: 10.1190/1.1441689.

Nabighian, M., 1997, Electromagnetic method in applied geophysics, Volume 1: Theory: SEG.

Plessix, R., 2009, Three-dimensional frequency-domain full-waveform inversion with an iterative solver: Geophysics, **74**, no. 6, WCC149–WCC157, doi: 10.1190/1.3211198.

Pyun, S., W. Son, and C. Shin, 2011, 3D acoustic wave form inversion in the Laplace domain using an iterative solver: Geophysical Prospecting, **59**, 386–399, doi: 10.1111/gpr.2011.59.issue-3.

Shin, C., and Y. Cha, 2008, Waveform inversion in the Laplace domain: Geophysical Journal International, **173**, 922–931, doi: 10.1111/gji.2008.173.issue-3.

Shin, C., and Y. Cha, 2009, Waveform inversion in the Laplace-Fourier domain: Geophysical Journal International, **177**, 1067–1079, doi: 10.1111/gji.2009.177.issue-3.

Shin, C., N. Koo, Y. Cha, and K. Park, 2010, Sequentially ordered single-frequency 2-D acoustic waveform inversion in the Laplace-Fourier domain: Geophysical Journal International, **181**, 935–950, doi: 10.1111/j.1365-246X.2010.04540.x.

Um, E., and D. Alumbaugh, 2007, On the physics of the marine controlled-source electromagnetic method: Geophysics, **72**, no. 2, WA13–WA26, doi: 10.1190/1.2432482.

Virieux, J., and S. Operto, 2009, An overview of full-waveform inversion in exploration geophysics: Geophysics, **74**, no. 6, WCC1–WCC26, doi: 10.1190/1.3238367.

DISCLAIMER